Large magnetoresistance in compensated semimetals $TaAs_2$ and $NbAs_2$

Zhujun Yuan,[1] Hong Lu,[1] Yongjie Liu,[2] Junfeng Wang,[2] and Shuang Jia[1,3,*]

[1]*International Center for Quantum Materials, School of Physics, Peking University, Haidian District, Beijing 100871, China*

[2]*Wuhan National High Magnetic Field Center, Huazhong University of Science and Technology, Wuhan 430074, China*

[3]*Collaborative Innovation Center of Quantum Matter, Beijing 100871, China*

(Received 22 February 2016; published 9 May 2016)

We report large magnetoresistance (MR) at low temperatures in single-crystalline nonmagnetic compounds $TaAs_2$ and $NbAs_2$. Both compounds exhibit parabolic-field-dependent MR larger than 5×10^3 in a magnetic field of 9 Tesla at 2 K. The MR starts to deviate from parabolic dependence above 10 T and intends to be saturated in 45 T for $TaAs_2$ at 4.2 K. The Hall resistance measurements and band structure calculations reveal their compensated semimetal characteristics. Their large MR at low temperatures is ascribed to an effect for compensation of electrons and holes with large mobilities. After discussing the MR for different samples of $TaAs_2$ and other semimetals, we found that the magnitudes of MR are strongly dependent on the samples' quality for different compounds.

DOI: 10.1103/PhysRevB.93.184405

I. INTRODUCTION

Magnetoresistance (MR) is defined as the change of material's resistance in magnetic fields ($MR \equiv \Delta\rho/\rho_{H=0}$). Recent studies on the single-crystalline semimetals including WTe_2 [1,2], Cd_3As_2 [3], $NbSb_2$ [4], LaSb [5], and MPn (M = Ta and Nb, Pn = P and As) [6–13] have revealed large MR varying from 1×10^3 to 2×10^4 in a magnetic field less than 10 Tesla (T) at low temperatures. Other metallic compounds such as $PtSn_4$ [14] and $PdCoO_2$ [15] with much higher carriers' density were reported to have large MR being 5.0×10^3 and 3.5×10^2 in a magnetic field of 14 T around 2 K, respectively. The MR for these compounds was described as "large," because the values are several orders of magnitude larger than that for normal metals such as copper [16]. But compared with the MR for the prototype semimetal element bismuth, which was reported to be as large as 1.6×10^7 at 4.2 K in 5 T [17], the MR for these nonmagnetic compounds is at least two orders of magnitude less.

Several mechanisms have been proposed to explain the large MR in nonmagnetic semimetals [18,19]. A classical two-band model predicts large parabolic-field-dependent MR in a compensated semimetal. A small difference of the electrons and holes densities (n and p) will cause the MR eventually saturated to a field-independent value [1,18,20]. Most of the compounds with large MR show a power law of field dependence very close to parabolic ($MR \propto H^2$). The compensation of electrons and holes was believed to occur in bismuth and graphite, while their MR was observed to be saturated in an intense magnetic field. On the other hand, the MR for WTe_2 and $NbSb_2$ is not saturated in a magnetic field as high as 60 and 32 T, respectively.

Some semimetals with large MR show the features that cannot be simply understood as a compensation effect of electrons and holes. The large MR for metallic $PtSn_4$ was reported as the result of ultrahigh mobility despite its large unbalanced electron and hole density [14]. The linear-field-dependence of the MR for Cd_3As_2 [3], Ag_2Se [21], and the recently reported Weyl semimetal TaAs family [6,8,9,22] is not expected for the compensation effect. The linear-field-dependent MR was understood as a quantum effect near the crossing point of the conduction and valence bands, which have linear energy dispersion when the magnetic field is beyond the quantum limit [23,24]. A classical effect of the spacial mobility fluctuation causes linear MR as well, which is more significant in polycrystalline samples [19]. Based on the studies of the large MR for these nonmagnetic compounds, the mechanisms underneath seem to be different from system to system. Exploring the semimetals which show large MR but crystallize in different structures will help to understand this complexity. Unfortunately, very limited semimetal compounds were reported to enact the forms of high-quality single crystals.

$TaAs_2$ and $NbAs_2$ belong to a group of transition metal dipnictides MPn_2 (M = V, Nb, Ta, Cr, Mo, and W, Pn = P, As, and Sb), which crystallize in an $OsGe_2$-type structure [25,26]. This structure has one crystallographic M site and two Pn sites in one unit cell [Fig. 1(a)]. Two Pn sites are quite distinct in their coordinations: one site is isolated from each other while the other site forms separated Pn-Pn dimers. The As-As bond lengths of the dimers in $TaAs_2$ and $NbAs_2$ are 2.42 Å and 2.44 Å, respectively [26,27], which are very close to the covalent radii 2.43 Å of the As-As dimer in tetramethyldiarsane [28]. Each tantalum and niobium atom is surrounded by six As atoms forming a trigonal prism with two additional As atoms outside the rectangular faces. The prisms are stacked along the crystallographic b direction through their trigonal faces to form the structure. A naive expectation for the electronic states of $NbAs_2$ and $TaAs_2$ is based on the simple Zintl concept [29,30]: a balanced state for valence electrons of $(Nb/Ta)_2^{5+}(As\text{-}As)^{4-}As_2^{6-}$ indicates an insulating state with a gap between the bands constructed by the bonding orbitals and antibonding orbitals of the As-As dimers. However, previous band structure calculations [30] suggested that $NbAs_2$ and $TaAs_2$ are semimetals instead of semiconductors. Although the Nb-Nb or Ta-Ta bonds with the bond length close to 3 Å are not considered in this oversimple

*gwljiashuang@pku.edu.cn

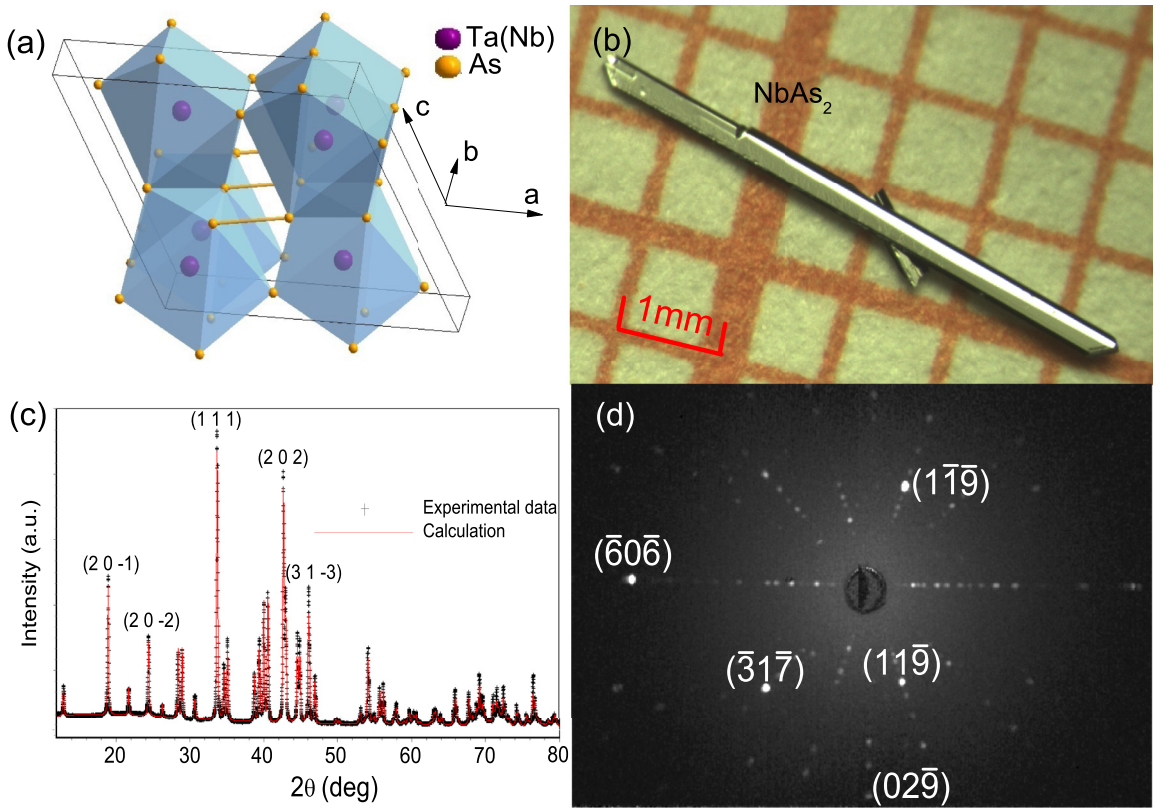

FIG. 1. (a) Crystal structure for Ta(Nb)As_2. (b) Photo of a single crystal of $NbAs_2$ on millimeter-grid paper. (c) Powder XRD spectrum for $TaAs_2$. The refinement results are close to those in Refs. [26] and [27]. (d) Laue backscattering diffraction pattern for a single crystal of $NbAs_2$.

Zintl concept, this rough estimation predicts the destitute density of states (DOS) for $TaAs_2$ and $NbAs_2$ near the Fermi level.

Physical properties for the MPn_2 family have not been extensively studied. $MoAs_2$ and WAs_2 were reported to be superconductors with the superconducting transition temperature (T_c) less than 1 K [30]. The semimetal behaviors and large, parabolic field-dependent MR at low temperatures in $NbSb_2$ were reported very recently [4]. The Sb atoms in $NbSb_2$ form the dimers with the Sb-Sb bond length of 2.71 Å as well. The band structure calculations for $NbSb_2$ show compensated, small electron and hole pockets near the Fermi level [4]. A electron hole compensation in $NbSb_2$ was suggested to be the reason for the large MR at low temperatures [4].

Due to highly volatile and toxic arsenic, single crystals of the transition metal diarsenides cannot be easily obtained via a regular flux growth as described in Refs. [4] and [2]. In this paper, we show that large single crystals of $NbAs_2$ and $TaAs_2$ can be grown via a chemical vapor transport (CVT) process. We found that these two compounds have large, parabolic-field-dependent MR at low temperatures. Based on the analysis of the electrical properties and band structure calculations, we believe that their large MR are due to an electron-hole compensation. After an analysis of the semimetals with large MR in previous reports, we found that

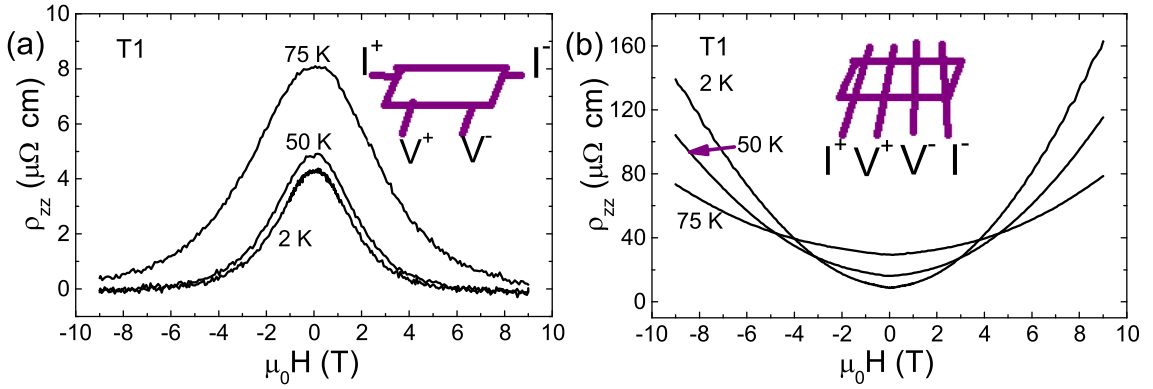

FIG. 2. (a) Measured "longitudinal MR" for the sample T1 of $TaAs_2$ when the contacts do NOT fully cross the sample as illustrated in the sketch. (b) Measured longitudinal MR for the same sample when the contacts fully cross the sample as illustrated in the sketch.

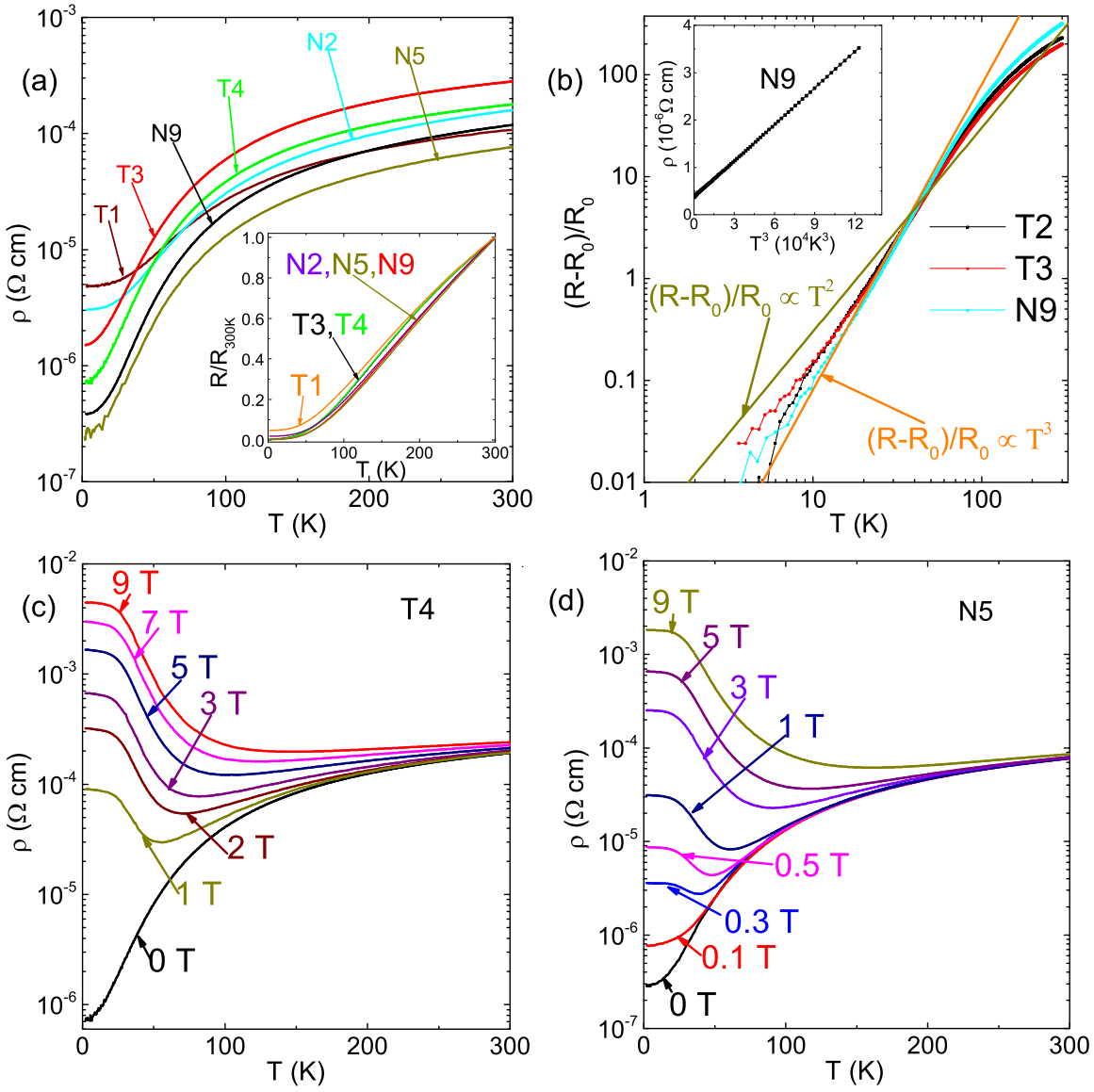

FIG. 3. (a) Temperature-dependent resistivity for different samples of $TaAs_2$ and $NbAs_2$ in a semilogarithmic plot (N for $NbAs_2$ and T for $TaAs_2$). Inset shows the $R(T)/R_{300K}$ versus T. (b) A double-logarithmic plot for the resistance and temperature. Inset shows the Resistivity versus T^3 for N9. (c, d) Temperature-dependent transversal resistivity for the samples T4 and N5 in different magnetic fields, respectively.

the values of MR are strongly dependent on the samples' quality. We believe that most of the large parabolic-field-dependent MR for compensated semimetals can be explained as a result of electron-hole balance.

II. EXPERIMENT

Single crystals of $TaAs_2$ and $NbAs_2$ were found as by-products when we tried to grow the single crystals of TaAs and NbAs via a CVT reaction method. Then we optimized the growth conditions in the previous report [27] for high-quality, large single crystals. Polycrystalline $TaAs_2$ and $NbAs_2$ was prepared by heating the stoichiometric amounts of elemental Ta/Nb and high-purity arsenic in evacuated silica ampules at 750°C for 2 days. Some redundant arsenic grains were always observed in the ampules after the synthesis. This phenomenon is consistent with the observation for the vacancy of arsenic atoms in $TaAs_2$ and $NbAs_2$ as described in Refs. [26] and [27]. The crystals of $TaAs_2$ were grown in a temperature gradient from 850°C (source) to 750°C (sink) for 7 days with the concentration of the agent $TaBr_5$ being 2.7mg/cm^3, while the crystals of $NbAs_2$ were grown in a temperature gradient from 775°C (source) to 700°C (sink) for 7 days with the concentration of the agent NbI_5 being 2.7 mg/cm^3. Blade-like crystals yielded in these conditions have a length of about 3–7 mm and a width of about 0.6 mm [Fig. 1(b)], while their residual resistivity ratio (RRR $= \rho_{300K}/\rho_{2K}$) is larger than 100 in transport measurements. CVT growth from the polycrystalline TaAs and NbAs as the sources instead of $TaAs_2$ and $NbAs_2$ and $TeCl_4$ (1.5 mg/cm^3) or TeI_4 (1.9 mg/cm^3) as the agent also yielded needle-like single crystals of $TaAs_2$ and $NbAs_2$ but their RRR is much smaller.

Powder x-ray diffraction (XRD) measurements were performed in a Rigaku MiniFlex 600 diffractometer. The

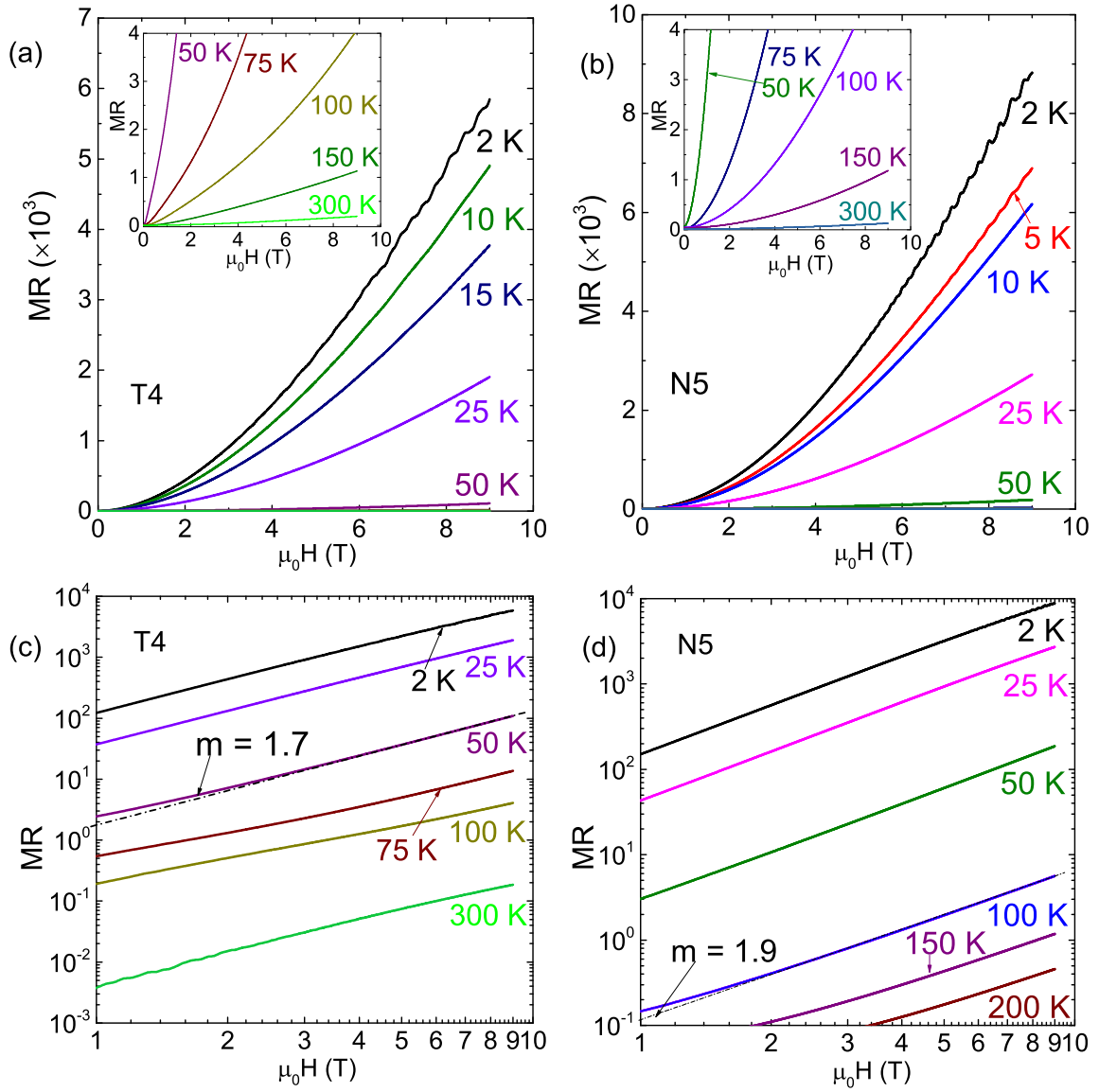

FIG. 4. (a, b) The MR versus magnetic field at different temperatures for the sample T4 and N5, respectively. Insets shows the MR at high temperatures. (c, d) The MR in double logarithmic plots for T4 and N5, respectively. MR $\propto H^m$ at low temperatures where $m = 1.7$ and 1.9 for T4 and N5, respectively.

refinements by using the Rietica Rietveld program confirm that the compounds crystallize in the structures of the space group C2/m, which is the same as previously reported [26]. The refined parameters are $a = 9.3372(2)$ Å, $b = 3.3847(1)$ Å, $c = 7.7711(2)$ Å, and $\beta = 119.638(1)^\circ$ for $TaAs_2$ and $a = 9.4017(2)$ Å, $b = 3.3947(1)$ Å, $c = 7.8212(2)$ Å, and $\beta = 119.531(1)^\circ$ for $NbAs_2$ [Fig. 1(c)]. Laue XRD measurements [Fig. 1(d)] on the single crystals were collected in a Photonic Science PSL-Laue backscattering system. The pattern shows that the long direction of the crystals is in the b direction, while the largest flat plane in the blade-like crystals is perpendicular to the (001) direction [Fig. 1(d)]. The transversal resistance and the Hall resistance were measured with a standard four-probe ac apparatus [31] in which the current is parallel to the b axis and the magnetic field is parallel to the (001) direction. The resistance and Hall data have been symmetrized to remove the effect of the misalignment of voltage wires ($\rho_{xx}(H) = \frac{\rho_{xx}(H)+\rho_{xx}(-H)}{2}$, $\rho_{yx}(H) = \frac{\rho_{yx}(H)-\rho_{yx}(-H)}{2}$). All the physical property characterizations were performed in a Quantum Design physical property measurement system (PPMS-9) over the temperature range from 1.9 to 300 K and in the magnetic fields up to 9 T.

Band structure calculations were performed by using the WIEN2K package [32] based on the full potential linearized augmented plane wave (LAPW) method [33] within local density approximation (LDA) [34]. The lattice constants were chosen from Ref. [26]. The values of the smallest atomic sphere radii in the unit cell (R_{mt}) were set to 2.48 and 2.22 Bohr for Ta and As in $TaAs_2$ and 2.43 and 2.20 Bohr for Nb and As in $NbAs_2$ by considering the difference of their nearest neighbor distances. The general gradient approximation (GGA) proposed by Perdew *et al.* [35] was used for the

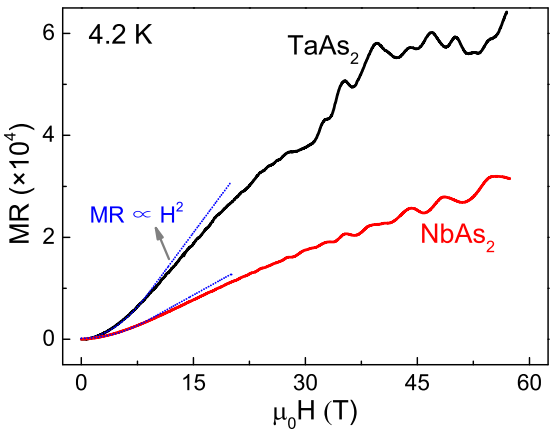

FIG. 5. MR for $TaAs_2$ and $NbAs_2$ in a pulsed magnetic field at 4.2 K.

exchange-correlation potential. A mesh of $21 \times 21 \times 21$ $\vec{k}$ points was selected for Brillouin zone integration with $R_{mt} * K_{max} = 7.0$ and Fermi surface plot, where K_{max} is the magnitude of the largest reciprocal lattice vector (K).

III. RESULTS

Before starting to describe the transport properties for $TaAs_2$ and $NbAs_2$, we present a misleading measurement result due to an improper experimental setup. Figures 2(a) and 2(b) show the measured resistivity for a same sample T1 with different contact setups as the insets, respectively, when the magnetic field is parallel with the current [H ∥ I]. The contacts attached the edge of the sample in the first setup, which is sometimes used for measuring Hall signal and transversal resistance at the same time. As shown in Fig. 2(a), a very large negative "longitudinal MR" occurs in the measurements for this setup. However, when the contacts fully cross the width in the second setup, the MR becomes a regular, small, positive profile [Fig. 2(b)]. We believe that the negative "longitudinal MR" is due to a magnetic-field-induced current jetting effect, which is commonly observed in high-mobility samples [16,36,37]. The current jetting effect must be seriously considered for measuring the longitudinal MR, especially for exploring the chiral anomaly in recently discovered Weyl semimetals [6,9].

Figure 3(a) shows a metallic profile for the temperature dependent resistivity for several representative samples for $TaAs_2$ and $NbAs_2$ in zero magnetic field. With a similar profile of linear-temperature-dependent resistivity above 100 K, the samples T3, T4, N5, and N9, which were grown by using $TaBr_5$ or NbI_5 as the transport agents have much smaller residual resistivity at 2 K than those of the samples T1 and N2, which were grown by using I_2 as the agent. Between 50 and 5 K, the samples with large RRR exhibit the R-T profiles with the relation $R(T) = R_0 + aT^n$ for $TaAs_2$ and $NbAs_2$. As shown in Fig. 3(b), n varies from 2.7 to 3.0 for five high-quality samples, which is different from a quadratic temperature dependent behavior for Fermi liquid. Due to the low resistance and relatively large measurement error, we cannot determine the power law below 5 K.

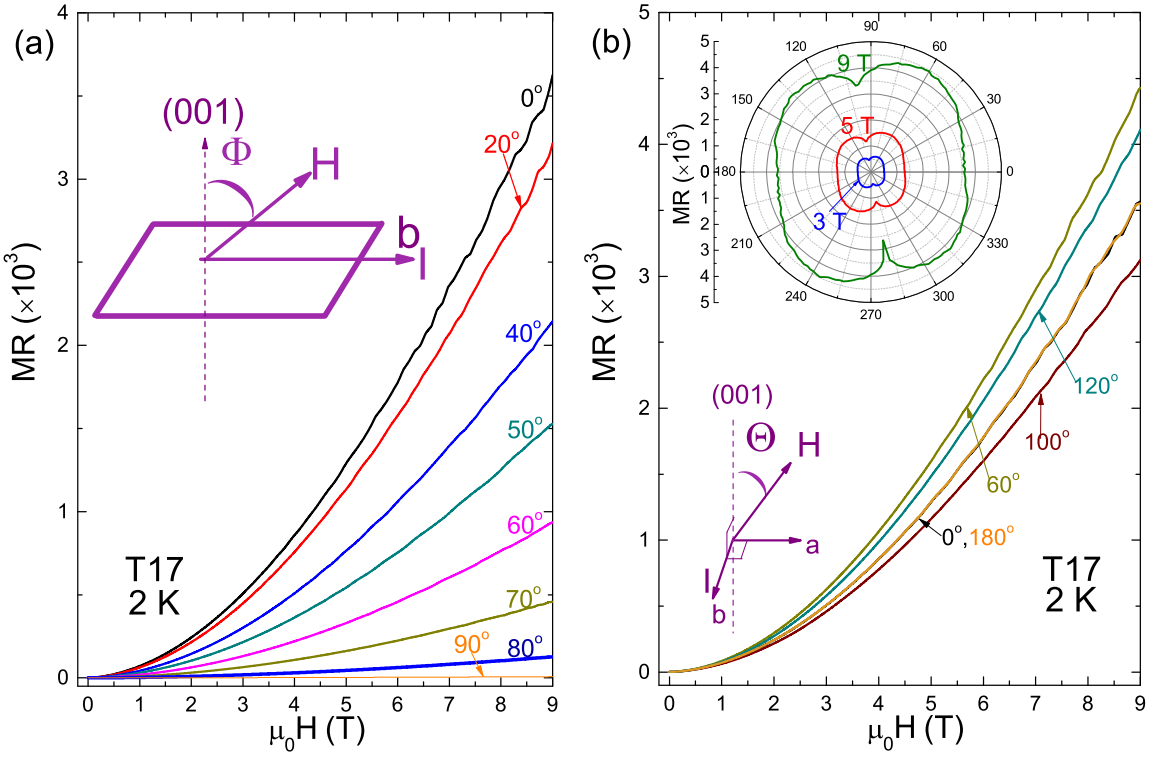

FIG. 6. (a) MR versus H at 2 K when H is tilted from (001) direction to b direction. Inset shows the sketch of the experimental setup. (b) Transversal MR versus H at 2 K when H is rotated in the plane perpendicular to b direction. Upper inset shows the angular dependent transversal MR at 2 K for H fixed in 3, 5, and 9 T. Lower inset shows the sketch of the transversal MR experimental setup. The angular dependence of the MR for $NbAs_2$ is similar as that for $TaAs_2$.

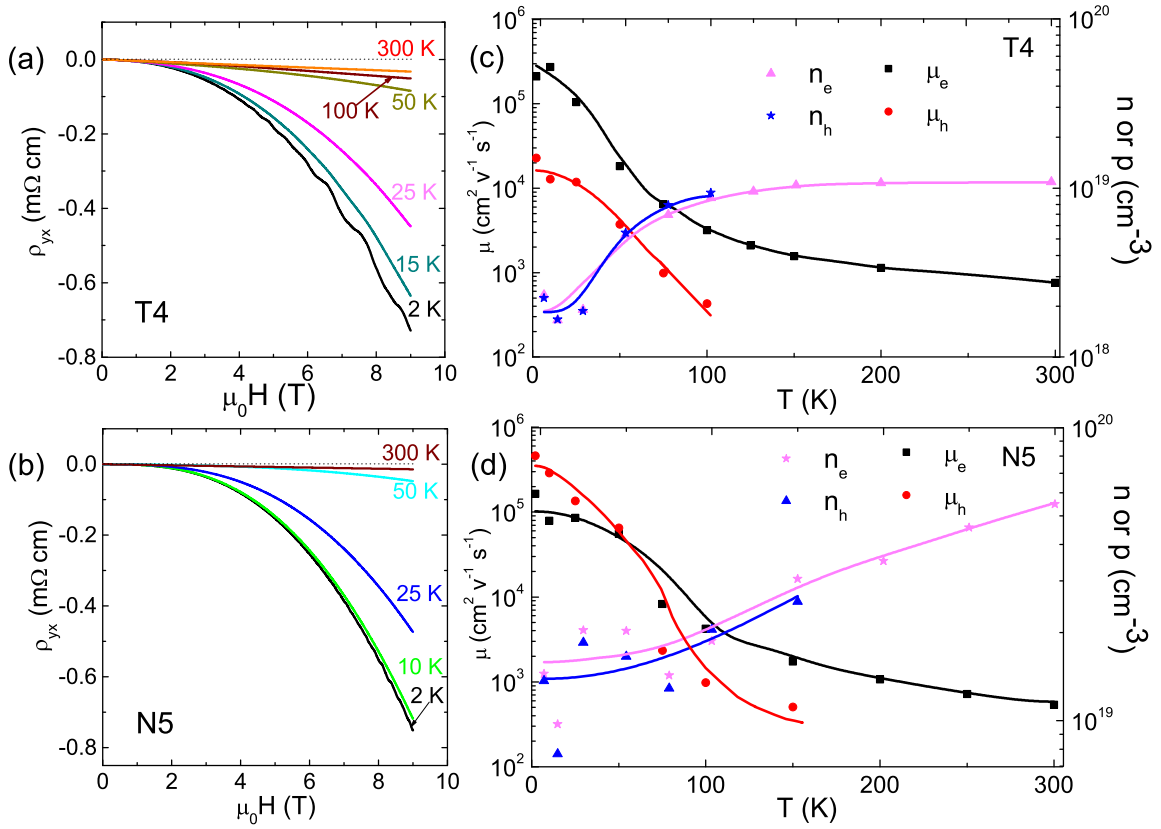

FIG. 7. (a, b) Field dependent Hall resistivity at different temperatures for the samples T4 and N5, respectively. (c, d) The fitting results for the electron and hole densities (n and p), and their mobilities (μ_e and μ_h) at different temperatures for T4 and N5, respectively. No hole information above 150 K is obtained in this measurement. The lines are guided by eyes.

When a magnetic field is applied to the samples T4 and N5 with large RRR, their resistivity at low temperatures significantly increases, while the increase at high temperatures is very limited [Figs. 3(c) and 3(d)]. The large difference of the MR at high and low temperatures leads $\rho(T)$ in a magnetic field showing a "transition" from a metallic profile at high temperatures to a semiconducting profile at low temperatures. This field-induced transition-like behavior is similar to the previously reported behavior in other semimetals [1,4,6,8,9,14,20].

Figures 4(a) and 4(b) show that the MR values decay three orders of magnitude from 2 to 100 K for T4 and N5. Below 5 K, the MR shows clear Shubnikov-de Haas (SdH) oscillations on the background of a parabolic profile. Although the MR changes significantly at different temperatures, it remains a clear power-law dependence with MR $\propto H^m$ where $m = 1.7$ and 1.9 for T4 and N5, respectively [Figs. 4(c) and 4(d)]. This power law is very close to a parabolic field dependence predicted by the two-band theory for identical compensated hole and electron densities [1,18,20]. The MR persists this power-law dependence but it is only 0.13 and 0.19 for N5 and T4 in 9 T at room temperature (300 K), respectively. We notice that some semimetals including bismuth and graphite [3,6,8,9,21,22,38,39] show their MR one to two orders of magnitude larger than those of $TaAs_2$ and $NbAs_2$ at room temperature. On the other hand, the MR values for T4 and N5 at room temperature are close to the reported values for WTe_2 [1], $NbSb_2$ [4], $PdCoO_2$ [15], and $PtSn_4$ [14].

In order to better understand the MR in higher magnetic fields, two samples were measured in a pulsed magnetic field as high as 55 T in National High Magnetic Lab in WuHan, China. Figure 5 shows the results for $TaAs_2$ and $NbAs_2$. The MR deviates from the quadratic field-dependent power law above 15 T. The MR for $TaAs_2$ shows strong, complicated SdH oscillations above 30 T and intends to be saturated at 45 T. Detail analysis on the saturations of MR in high magnetic field will be presented in the future.

Figure 6 shows the MR when the magnetic field is tilted in different directions while the current is always along b direction. In order to minimize the current jetting effect, the sample T17 was prepared to be long, thin bars with four contacts fully cross their width in this measurement. When the field direction is tilted from that parallel to the (001) direction to b direction, the MR drops rapidly [Fig. 6(a)]. Such large difference between the longitudinal and transversal MR is also observed in WTe_2 [1] and $NbSb_2$ [4]. On the other hand, the transversal MR changes small when the magnetic field is rotated in the plane perpendicular to b direction. Figure 6(b) shows that the minimal of the transversal MR occur when the field is close to the a direction ($\Theta = 280^\circ$ and 100°). The polar plot for the MR in the inset of Fig. 6(b) shows a twofold-rotation symmetric pattern,

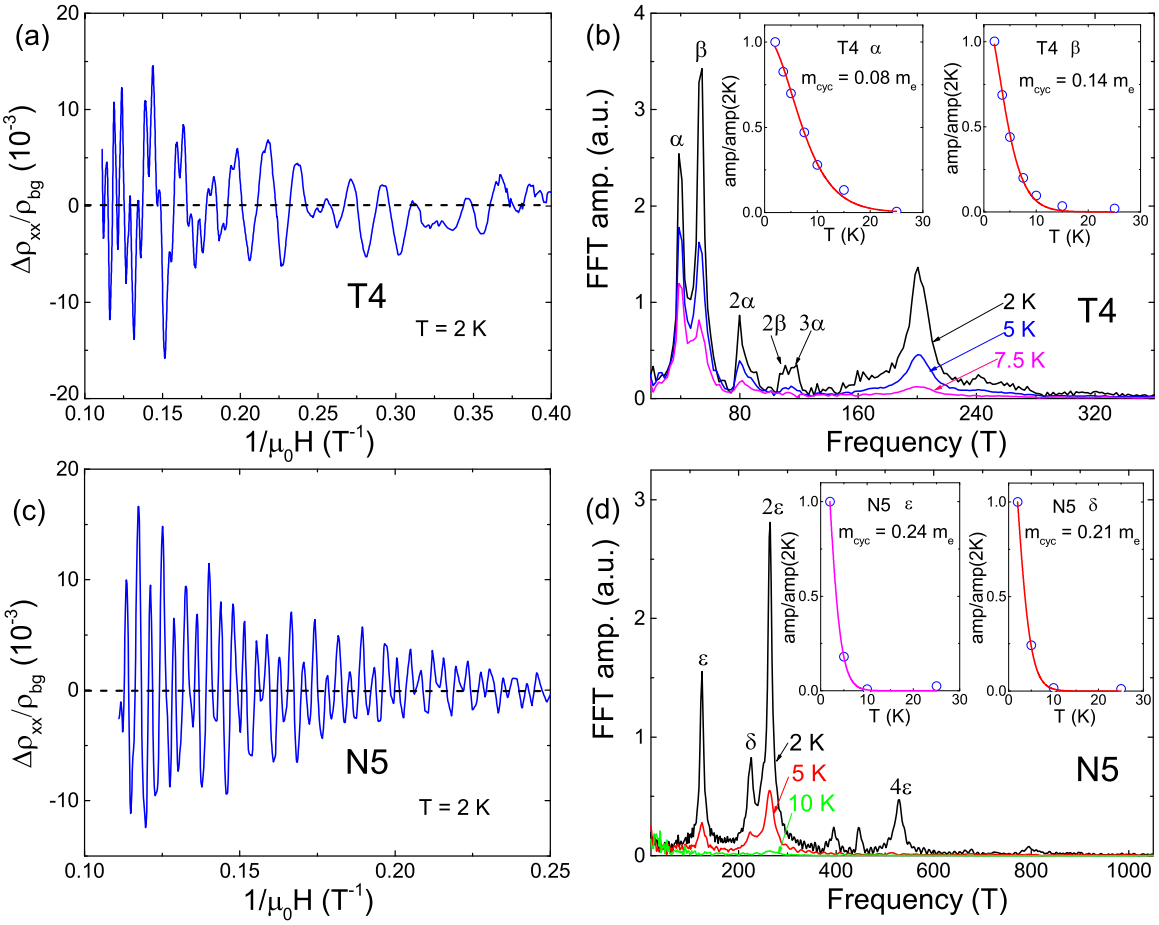

FIG. 8. (a, c) Oscillatory part of the resistivity ratio $\delta\rho_{xx}/\rho_{bg}$ versus $1/\mu_0 H$ for the samples T4 and N5 at 2 K, respectively, where ρ_{bg} is the nonoscillation background of ρ_{xx}. Insets show the (b, d) FFT spectra for T4 and N5 at different temperatures. Insets show the fitting of the amplitude of the SdH oscillations with respect to temperature yields the cyclotron electron mass for the main frequencies for T4 and N5, respectively.

which is consistent with the monoclinic crystal structure. The cusp in MR for $\Theta = 280^\circ$ and 100° may be due to special Fermi surface geometry [38] or relatively large sampling interval.

Hall measurements provide information about the carriers for $TaAs_2$ and $NbAs_2$. Figures 7(a) and 7(b) show that the Hall resistivity (ρ_{yx}) is negative and linear dependent to the magnetic field when T $\geqslant$ 125 K and 200 K for T4 and N5, respectively. At low temperatures, ρ_{yx} apparently deviates from the linear-field dependence, which indicates two types of carriers. We found that the Hall conductivity (σ_{xy}) can be well-fitted by the two-carrier model from the two-band theory [40],

$$\sigma_{xy} = [n_h\mu_h^2\frac{1}{1+(\mu_h H)^2} - n_e\mu_e^2\frac{1}{1+(\mu_e H)^2}]eH, \qquad (1)$$

where $\sigma_{xy} = \frac{\rho_{yx}}{\rho_{yx}^2+\rho_{xx}^2}$, n_e (n_h), and μ_e (μ_h) denote the carrier concentrations and mobilities for electrons (holes), respectively. The Hall conductivity for $NbAs_2$ changes from positive to negative at low temperatures (the datum are not showing here). The fitting results show close n and p at low temperatures [Figs. 7(c) and 7(d)]. At high temperature range, the hole contributions to the Hall signals are negligible due to its rapidly decreased mobility, and the data can be well fitted by an one-band model. The mobilities at 2 K are about 1×10^5 $cm^2V^{-1}s^{-1}$ for electrons and holes for both $TaAs_2$ and $NbAs_2$. At room temperature, μ_e drops to the order of 5×10^2 $cm^2V^{-1}s^{-1}$ for both samples. The Hall measurements reveal that $TaAs_2$ and $NbAs_2$ are compensated semimetals with large mobilities of electrons and holes at low temperatures.

The SdH oscillations in the field-dependent resistivity for $TaAs_2$ and $NbAs_2$ were extracted via subtracting the nonoscillation background (ρ_{bg}) and dividing by the background at low temperatures (Fig. 8). The SdH oscillations with respect to $1/H$ form complicated patterns which obviously come from multiple frequencies. Fast Fourier transform (FFT) analysis reveals that the samples T4 has two main frequencies about $\alpha = 39(3)$ T and $\beta = 54(3)$ T and N5 has two main frequencies about $\epsilon = 124(3)$ T and $\delta = 224(3)$ T, while the double and higher harmonic frequencies of the main frequencies were observed as well (Figs. 8(b) and 8(d)). The origin of frequency about 200 T for T4 is not clear. The complete identification of the entire Fermi surface from quantum oscillation is left for future work.

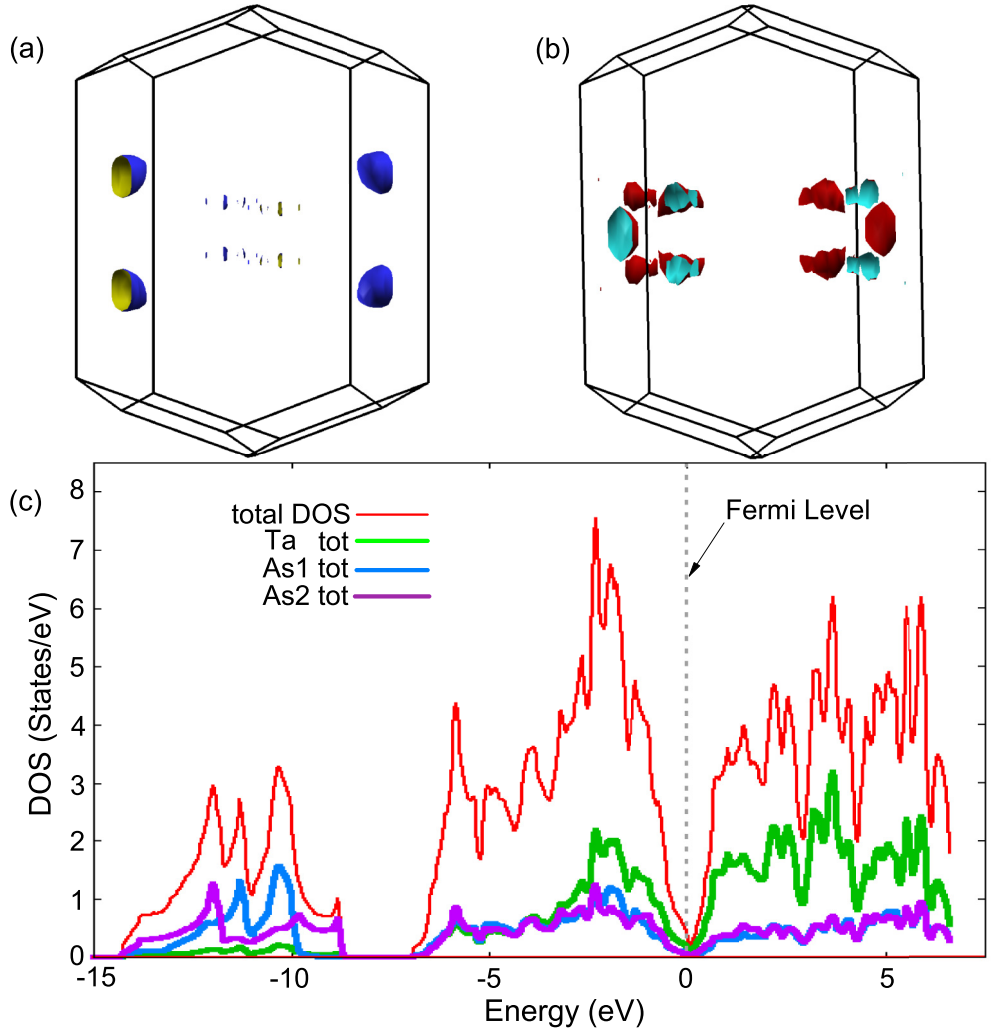

FIG. 9. (a, b) Fermi Surfaces of electron and hole pockets for $TaAs_2$ in its primitive Brillouin zone, respectively. (c) The total and partial DOS for $TaAs_2$.

The existence of multiharmonic frequencies indicates a long transport lifetime for both compounds in accordance with their high mobilities. In order to obtain the cyclotron mass for the main frequencies, we fitted FFT amplitude ratio amp/amp($2K$) versus temperature for main frequencies of T4 and N5, respectively [Figs. 8(b) and 8(d)]. Using the fitting formula [41],

$$\frac{\text{amp}}{\text{amp}(2K)} \propto \frac{2\pi^2 k_B T/\hbar\omega_c}{\sinh(2\pi^2 k_B T/\hbar\omega_c)}, \quad (2)$$

where k_B is Boltzmann constant, cyclotron frequency $\omega_c = e\bar{B}/m_{\text{cyc}}$, m_{cyc} is cyclotron mass, and $\bar{B}$ is the effective magnetic field in fitting range (from 1.6 T to 9 T), we got m_{cyc} equals to 0.08(2) m_e, 0.14(3) m_e, 0.24(3) m_e, and 0.21(3) m_e for α, β, ϵ, and δ, respectively. The m_{cyc} for frequency about 200 T for T4 equals to 0.18(3) m_e. Further experiments accompanied by accurate band structure calculations are needed to address the pockets related to these SdH oscillations.

IV. DISCUSSION

The calculated band structures for $TaAs_2$ and $NbAs_2$ are consistent with their compensated semimetal characteristics. Figures 9(a) and 9(b) show the Fermi surface mapping in which only one valence and conduction bands intersect the Fermi level, respectively. Small, ellipse-like electron and hole pockets appear at the boundary of the primitive Brillouin zone. The DOS at Fermi level is very close to the minimum in the spectrum [Fig. 9(c)]. The results for $TaAs_2$ and $NbAs_2$ are similar as those in Ref. [28] and the band structure for $NbSb_2$ [4]. Since the Fermi surface is complicated with several different electron and hole pockets, the identification of the frequencies for the SdH oscillations with the extremal surface areas needs further elaborations.

We next discuss the sample and temperature dependence for the large MR for $TaAs_2$. Table I shows that the values of RRR and MR are strongly dependent on the transport agents using in the growth. Although the MR changes four orders of magnitude for different samples, it follows the same power law of MR $= bH^m$, where $m = 1.7 \pm 0.1$ for all the samples (Fig. 10). On the other hand, the coefficient b seems to follow a

TABLE I. RRR and MR for different samples of $TaAs_2$ and $NbAs_2$ grown by using different transport agents.

Sample	Transport agent	RRR	MR at 2 K in 9 T
N2	I_2	53.6	332
N5	NbI_5: 75 mg	317	8.8×10^3
N9		313	7.4×10^3
T1	I_2	24.0	95.7
T2	$TaBr_5$: 75 mg	224	3.2×10^3
T3		198	2.0×10^3
T4		270	5.8×10^3
T17		218	3.6×10^3
T5	$TaBr_5$: 74 mg	44.0	315
T6	and $TeBr_4$: 4.7mg	42.4	285
T7		41.5	268
T8	$TaBr_5$: 74 mg	15.6	44.4
T9	and $TeBr_4$: 11.4mg	17.3	53.8
T10		18.6	55.1
T11	$TaBr_5$: 74 mg	33.0	168
T13	and $TeBr_4$: 22.3 mg	38.4	208
T14	$TeBr_4$: 35 mg	2.30	0.093
T15		2.33	0.064
T16		2.42	0.258

All the samples come from nine batches with different transport agents. The growth conditions are the same as described in Sec. II.

power law of $b \propto \mathrm{RRR}^q$ where $q = 1.6$ for all $TaAs_2$ samples. This power law relation for the RRR and b results in the giant difference for the MR for the samples with different qualities. The dependence of the MR and RRR on the transport agents is likely due to the doping effect of the impurity from the transport agents, such as tellurium atoms on the As site, or the arsenic deficiency described in Ref. [27]. Similar significant drop of large MR due to chemical doping has been observed in WTe_2 [42].

In order to better understand the electron scattering in different samples, the MR at 2 K for different samples is plotted in a modified Kohler plot [Fig. 10(c)]. Considering the large uncertainty of the dimensions for the samples, we chose $(\mu_0 H \times \mathrm{RRR})^{1.7}$ instead of $(\mu_0 H/\rho_0)^{1.7}$ in the plot. We notice that the curves for the samples with relatively small MR (<100) cluster together, while the curves for the three samples of T2, T3 and T4 with large MR (>1000) clearly deviate from the cluster. A plausible explanation is that the impurity induced electron scattering dominates the transport behaviors in a magnetic field for those samples with small RRR. For high-quality samples such as T2, T3, and T4, the scattering process in a magnetic field is strongly dependent on the samples. A modified Kohler plot for the MR versus $(\mu_0 H/\rho_0)^{1.7}$ for the sample T4 at different temperatures is shown in Fig. 10(d). The curves do not fall into a same region

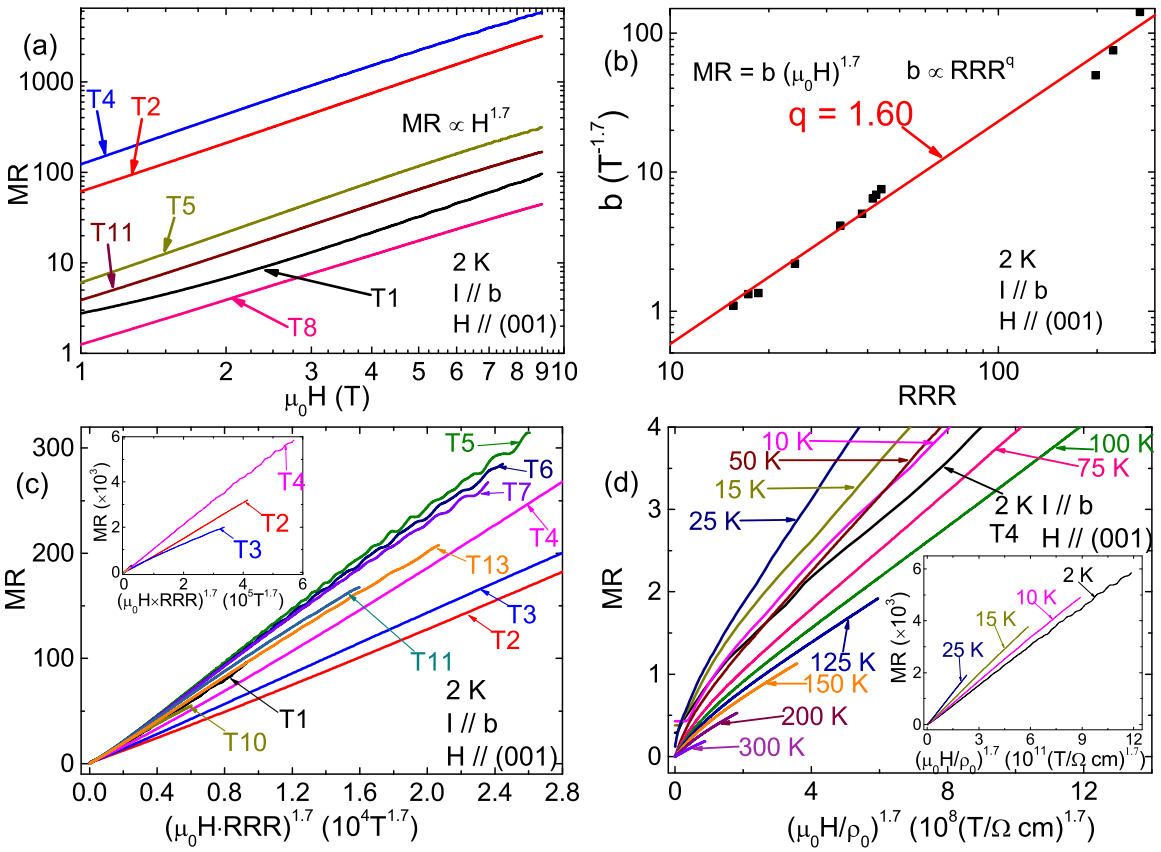

FIG. 10. (a) MR versus magnetic field for different samples of $TaAs_2$ at 2 K in a double-logarithmic plot. (b) Coefficient b (MR $= b \times H^{1.7}$) versus RRR for different samples of $TaAs_2$ in a double-logarithmic plot. The red line is the fitting line of the order of 1.6. (c) Modified Kohler plot for different samples of $TaAs_2$ at 2 K. Inset shows the Kohler plot for the samples T2, T3, and T4 at 2K in different range. (d) Kohler plot for the sample T4 at different temperatures using $MR = F[H/\rho(0)] \propto [H/\rho(0)]^{1.7}$. Inset shows the same Kohler plot of (d) in different range.

TABLE II. Summarized parameters for the semimetals showing large parabolic MR at low temperatures.

Semimetal	μ ($cm^2V^{-1}s^{-1}$)	RRR	MR	Reference
Bi	N.A	476	1.6×10^7 at 4.2 K 5 T	[17]
Bi	1.1×10^7	150	2×10^4 at 2 K 0.5 T	[38]
Bi	3×10^6	40	1.1×10^4 at 4.2 K and 1.8 T	[50]
Graphite	1.0×10^6	37	8.3×10^3 at 4.2 K and 2.3 T	[51]
WTe_2	1×10^5	1256	3.1×10^3 at 1.2 K and 10 T	[2]
WTe_2	5×10^4	370	4.5×10^3 at 4.5 K and 14.7 T	[1]
$TaAs_2$	2.1×10^5	270	5.8×10^3 at 2 K and 9 T	Current paper
$NbAs_2$	1.6×10^5	317	8.8×10^3 at 2 K and 9 T	Current paper
$NbSb_2$	N.A	450	8.8×10^3 at 2 K and 9 T	[4]
Cd	N.A	4.0×10^4	1×10^5 at 1.4 K and 2.5 T	[52]

The mobility data were collected from the fitting of two-carrier-model in the literatures.

at any temperatures. Since the mobilities of the electrons and holes have different temperature dependence, the violation of the Kohler's rule is not unexpected.

We list the parameters for the compensated semimetals with large, parabolic-field-dependent MR in Table II. All the semimetals with large MR have their main-carrier mobilities much larger than 1 $m^2V^{-1}s^{-1}$. It seems that the MR for all the semimetals is positively correlated with their RRR and mobilities, despite the large difference of the band structures and carrier densities.

Finally, we discuss the saturation of the MR for the compensated semimetals. The parabolic MR for WTe_2 does not show any sign of saturation in a magnetic field up to 60 T, which is believed to be due to a prefect balance of the electron and hole pockets [1,2]. As far as we know, the saturations of the transversal MR for compensated semimetals have only been observed for bismuth [43] and graphite [44], which have small quantum limits less than 10 T. In such high field, the quantum effect may affect the MR significantly different from the classical behaviors. The MR for $TaAs_2$ intends to be saturated in 45 T while its quantum limit is about 50 T. Whether a quantum effect also affects the saturation of the MR for semimetal need further measurements for other semimetals in strong magnetic field.

V. CONCLUSION

To conclude, we grew large single crystals of $NbAs_2$ and $TaAs_2$ via a CVT process. These two compounds are compensated semimetals with large, parabolic-field-dependent MR at low temperatures. We believe that most of the large, parabolic MR for the compensated semimetals can be explained as a result of electron-hole balance.

Note: We noticed several related works in arXiv [45–49] when we prepared this draft.

ACKNOWLEDGMENTS

We thank Cheng-Long Zhang for pointing out the current jet problem in the negative longitudinal magnetoresistance. We thank Yongkang Luo for helpful discussion. He pointed out the problem of the cyclotron mass fitting in the old version. We thank Yuan Li and Ji Feng for using their instruments. This project is supported by National Basic Research Program of China (Grants No. 2013CB921901 and No. 2014CB239302).

[1] M. N. Ali, J. Xiong, S. Flynn, J. Tao, Q. D. Gibson, L. M. Schoop, T. Liang, N. Haldolaarachchige, M. Hirschberger, N. P. Ong, and R. J. Cava, Large, nonsaturating magnetoresistance in WTe_2, Nature **514**, 205 (2014).

[2] Z. Zhu, X. Lin, J. Liu, B. Fauqué, Q. Tao, C. Yang, Y. Shi, and K. Behnia, Quantum Oscillations, Thermoelectric Coefficients, and the Fermi Surface of Semimetallic WTe_2, Phys. Rev. Lett. **114**, 176601 (2015).

[3] T. Liang, Q. Gibson, M. N. Ali, M. Liu, R. J. Cava, and N. P. Ong, Ultrahigh mobility and giant magnetoresistance in the dirac semimetal Cd_3As_2, Nat. Mater. **14**, 280 (2014).

[4] K. Wang, D. Graf, L. Li, L. Wang, and C. Petrovic, Anisotropic giant magnetoresistance in $NbSb_2$, Sci. Rep. **4**, 7328 (2014).

[5] F. F. Tafti, Q. D. Gibson, S. K. Kushwaha, N. Haldolaarachchige, and R. J. Cava, Resistivity plateau and extreme magnetoresistance in LaSb, Nature Phys. **12**, 272 2015.

[6] C.-L. Zhang, S.-Y. Xu, I. Belopolski, Z. Yuan, Z. Lin, B. Tong, G. Bian, N. Alidoust, C.-C. Lee, S.-M. Huang, T.-R. Chang, G. Chang, C.-H. Hsu, H.-T. Jeng, M. Neupane, D. S. Sanchez, H. Zheng, J. Wang, H. Lin, C. Zhang, H.-Z. Lu, S.-Q. Shen, T. Neupert, M. Z. Hasan, and S. Jia, Observation of the adler-bell-jackiw chiral anomaly in a weyl semimetal, Nat. Commun. **7**, 10735 (2016).

[7] Yongkang Luo, N. J. Ghimire, M. Wartenbe, Hongchul Choi, M. Neupane, R. D. McDonald, E. D. Bauer, Jianxin Zhu, J. D. Thompson, and F. Ronning, Electron-hole compensation effect between topologically trivial electrons and nontrivial holes in NbAs, Phys. Rev. B **92**, 205134, (2015).

[8] C. Shekhar, A. K. Nayak, Y. Sun, M. Schmidt, M. Nicklas, I. Leermakers, U. Zeitler, Y. Skourski, J. Wosnitza, Z. Liu, Y. Chen, W. Schnelle, H. Borrmann, Y. Grin, C. Felser, and B. Yan, Extremely large magnetoresistance and ultrahigh mobility in the topological weyl semimetal candidate NbP, Nature Phys. **11**, 645 (2015).

[9] C. Zhang, C. Guo, H. Lu, X. Zhang, Z. Yuan, Z. Lin, J. Wang, and S. Jia, Large magnetoresistance over an extended temperature regime in monophosphides of tantalum and niobium, Phys. Rev. B **92**041203 (2015).

[10] Xiaochun Huang, Lingxiao Zhao, Yujia Long, Peipei Wang, Dong Chen, Zhanhai Yang, Hui Liang, Mianqi Xue, Hongming Weng, Zhong Fang, Xi Dai, and Genfu Chen, Observation of the Chiral-Anomaly-Induced Negative Magnetoresistance in 3d Weyl Semimetal TaAs, Phys. Rev. X **5**, 031023 (2015).

[11] Z. Wang, Y. Zheng, Z. Shen, Y. Lu, H. Fang, F. Sheng, Y. Zhou, X. Yang, Y. Li, C. Feng, and Z.-A. Xu, Helicity protected ultrahigh mobility weyl fermions in NbP, Phys. Rev. B **93**, 121112 (2016).

[12] X. Yang, Y. Liu, Z. Wang, Y. Zheng, and Z. Xu, Chiral Anomaly Induced Negative Magnetoresistance in Topological Weyl Semimetal NbAs, arXiv:1506.03190 (2015).

[13] B. Q. Lv, H. M. Weng, B. B. Fu, X. P. Wang, H. Miao, J. Ma, P. Richard, X. C. Huang, L. X. Zhao, G. F. Chen, Z. Fang, X. Dai, T. Qian, and H. Ding, Experimental Discovery of Weyl Semimetal TaAs, Phys. Rev. X **5**, 031013, (2015).

[14] E. Mun, H. Ko, G. J. Miller, G. D. Samolyuk, S. L. Bud'ko, and P. C. Canfield, Magnetic field effects on transport properties of $PtSn_4$, Phys. Rev. B **85**, 035135 (2012).

[15] H. Takatsu, J. J. Ishikawa, S. Yonezawa, H. Yoshino, T. Shishidou, T. Oguchi, K. Murata, and Y. Maeno, Extremely Large Magnetoresistance in the Nonmagnetic Metal $PdCoO_2$, Phys. Rev. Lett. **111**, 056601 (2013).

[16] A. B. Pippard, *Magnetoresistance in Metals* (Cambridge University Press, Cambridge, 2009).

[17] P. B. Alers, and R. T. Webber, The magnetoresistance of bismuth crystals at low temperatures, Phys. Rev. **91**, 1060 (1953).

[18] J. M. Ziman, *Electrons and Phonons. The Theory of Transport Phenomena in Solids* (Oxford University Press, Oxford, 2001).

[19] M. M. Parish, and P. B. Littlewood, Nonsaturating magnetoresistance in heavily disordered semiconductors, Nature **426**, 162 (2003).

[20] X. Du, S. Tsai, D. L. Maslov, and A. F. Hebard, Metal-Insulator-Like Behavior in Semimetallic Bismuth and Graphite, Phys. Rev. Lett. **94**, 166601 (2005).

[21] C. Zhang, H. Liu, T. Chang, S. Xu, W. Hua, H. Jiang, Z. Yuan, J. Sun, H. T. Jeng, M. Z. Hasan, X. C. Xie, and S. Jia, Ultraquantum magnetoresistance in single-crystalline β-Ag_2Se, arXiv:1502.02324 (2015).

[22] N. J. Ghimire, Y. Luo, M. Neupane, D. J. Williams, E. D. Bauer, and F. Ronning, Magnetotransport of single crystalline NbAs, J. Phys.: Condens. Matter **27**, 152201 (2015).

[23] A. A. Abrikosov, Quantum magnetoresistance, Phys. Rev. B **58**, 2788 (1998).

[24] A. A. Abrikosov, Quantum linear magnetoresistance, Europhys. Lett. **49**, 789 (2000).

[25] F. Hulliger, New representatives of the $NbAs_2$ and $ZrAs_2$ structures, Nature **204**, 775 (1964).

[26] W. Bensch and W. Heid, $NbAs_2$, Acta Crystallogr. Sec. C **51**, 2205 (1995).

[27] G. S. Saini, L. D. Calvert, and J. B. Taylor, Preparation and characterization of crystals of Mx- and Mx_2-type arsenides of niobium and tantalum, Can. J. Chem. **42**, 630 (1964).

[28] O. Mundt, H. Riffel, G. Becker, and A. Simon, Molekül- und kristallstruktur des tetramethyldiphosphans und-diarsans (element-element-bindungen; 4), Zeitschrift fär Naturforschung B **43**, 952, (1988).

[29] R. Nesper, The zintl-klemm concept – a historical survey, Z. Anorg. Allg. Chem. **640**, 2639 (2014).

[30] P. Alemany and S. Alvarez, Theoretical study of bonding and electrical conductivity in compounds with the $NbAs_2$ structure, Inorg. Chem. **31**, 3007 (1992).

[31] R. R. Heikes, and R. W. Ure, *Thermoelectricity: Science and Engineering* (Interscience Publishers, London, 1961).

[32] *WIEN2k, An Augmented Plane Wave + Local Orbitals Program for Calculating Crystal Properties*. Karlheinz Schwarz, Techn. Universitat Wien, Austria (2001).

[33] M. Weinert, E. Wimmer, and A. J. Freeman, Total-energy all-electron density functional method for bulk solids and surfaces, Phys. Rev. B **26**, 4571 (1982).

[34] J. P. Perdew, and Y. Wang, Accurate and simple analytic representation of the electron-gas correlation energy, Phys. Rev. B **45**, 13244 (1992).

[35] J. P. Perdew, K. Burke, and M. Ernzerhof, Generalized Gradient Approximation Made Simple, Phys. Rev. Lett. **77**, 3865 (1996).

[36] J. Hu, T. F. Rosenbaum, and J. B. Betts, Current Jets, Disorder, and Linear Magnetoresistance in the Silver Chalcogenides, Phys. Rev. Lett. **95**, 186603 (2005).

[37] N. A. Porter, and C. H. Marrows, Linear magnetoresistance in *n*-type silicon due to doping density fluctuations, Sci. Rep. **2** (2012).

[38] Z. Zhu, A. Collaudin, B. Fauque, W. Kang, and K. Behnia, Field-induced polarization of dirac valleys in bismuth, Nature Phys. **8**, 89 (2011).

[39] D. E. Soule, Magnetic field dependence of the hall effect and magnetoresistance in graphite single crystals, Phys. Rev. **112**, 698 (1958).

[40] C. M. Hurd, *The Hall Effect in Metals and Alloys* (Cambridge University Press, Cambridge, 1972).

[41] H. Murakawa, M. S. Bahramy, M. Tokunaga, Y. Kohama, C. Bell, Y. Kaneko, N. Nagaosa, H. Y. Hwang, and Y. Tokura, Detection of berrys phase in a bulk rashba semiconductor, Science **342**, 1490 (2013).

[42] Steven Flynn, Mazhar Ali, and R. J. Cava, The effect of dopants on the magnetoresistance of WTe_2, arXiv:1506.07069 (2015).

[43] B. Fauqué, B. Vignolle, C. Proust, J.-P. Issi, and K. Behnia, Electronic instability in bismuth far beyond the quantum limit, New J. Phys. **11**, 113012 (2009).

[44] B. Fauqué, D. LeBoeuf, B. Vignolle, M. Nardone, C. Proust, and K. Behnia, Two Phase Transitions Induced by a Magnetic Field in Graphite, Phys. Rev. Lett. **110**, 266601 (2013).

[45] D. Wu, J. Liao, W. Yi, X. Wang, P. Li, H. Weng, Y. Shi, Y. Li, J. Luo, X. Dai, and Z. Fang, Giant semiclassical magnetoresistance in high mobility $TaAs_2$ semimetal, Appl. Phys. Lett. **108**, 042105 (2016).

[46] Y. Wang, Q. Yu, and T. Xia, Resistivity plateau and extremely large magnetoresistance in $NbAs_2$ and $TaAs_2$, arXiv:1601.04239 (2016).

[47] Y. Luo, R. D. McDonald, P. F. S. Rosa, B. Scott, N. Wakeham, N. J. Ghimirey, E. D. Bauer, J. D. Thompsonz, and F. Ronning, Anomalous magnetoresistance in $TaAs_2$, arXiv:1601.05524 (2016).

[48] B. Shen, X. Deng, G. Kotliar, and N. Ni, Fermi surface topology and negative magnetoresistance observed in centrosymmetric $NbAs_2$ semimetal, arXiv:1602.01795 (2016).

[49] Y. Li, L. Li, J. Wang, T. Wang, X. Xu, C. Xi, C. Cao, and J. Dai, Field-induced resistivity plateau and unsaturated

negative magnetoresistance in topological semimetal $TaSb_2$, arXiv:1601.02062 (2016).

[50] C. G. Grenier, J. M. Reynolds, and J. R. Sybert, Electron transport phenomena in bismuth at liquid-helium temperatures, Phys. Rev. **132**, 58 (1963).

[51] D. E. Soule, Analysis of galvanomagnetic de haas-van alphen type oscillations in graphite, Phys. Rev. **112**, 708 (1958).

[52] O. P. Katyal, and A. N. Gerritsen, Investigation of hall resistivity and magnetoresistance of cadmium and cadmium-zinc crystals, Phys. Rev. **178**, 1037 (1969).